Applied Bionics and Biomechanics 9 (2012) 333–345
DOI 10.3233/ABB-2012-0064
IOS Press

Robotic pectoral fin thrust vectoring using weighted gait combinations

John S. Palmisano[a,*], Jason D. Geder[b], Ravi Ramamurti[b], William C. Sandberg[b,c] and Banahalli Ratna[a]
[a]*Center for Biomolecular Science and Engineering at the Naval Research Laboratory in Washington, DC, USA*
[b]*Laboratory for Computational Physics and Fluid Dynamics at the Naval Research Laboratory in Washington, DC, USA*
[c]*Science Applications International Corp, Oration, Mclean, VA, USA*

Abstract. A method was devised to vector propulsion of a robotic pectoral fin by means of actively controlling fin surface curvature. Separate flapping fin gaits were designed to maximize thrust for each of three different thrust vectors: forward, reverse, and lift. By using weighted combinations of these three pre-determined main gaits, new intermediate hybrid gaits for any desired propulsion vector can be created with smooth transitioning between these gaits. This weighted gait combination (WGC) method is applicable to other difficult-to-model actuators. Both 3D unsteady computational fluid dynamics (CFD) and experimental results are presented.

Keywords: CFD, controlled curvature, pectoral fin, weighted gait combination, thrust vectoring

1. Introduction

FIN flapping is a locomotor motion useful for both stability control and propulsion. Many animals use flapping as the primary means of locomotion, including birds, fish, marine mammals, and insects. By flapping a fin, wing, or flipper, these animals are capable of many amazing feats not yet achieved with man-made machines. If biomimetically flapping robots with higher efficiency, improved control, greater payload capacity, and higher speeds are ever to be realized, the flapper must be well understood.

In the majority of the literature, researchers have treated flappers as rigid plates with basic sinusoidal control laws to simplify modeling. However, those mathematical approximations and mechanical simplifications result in reduced propulsive performance as shown by CFD modeling [1, 2], theoretical modeling [3], and by biological analysis [4]. "Although many models of fish fin function treat the fins as rigid flat plates with constant area, fish fins are anything but rigid and their flexibility is important for vectoring forces and for thrust production [4]." The flapper is a complex shape-changing surface (see Figs. 1 and 4): surface area, surface curvature, angle of attack, aspect ratio, leading edge curvature, and other major parameters are important contributors to thrust vectoring, with the added complexity that each of these continuously change throughout the flap stroke [1].

Since the importance of each major flapping fin parameter is now relatively well-understood, forward thrust can be determined given any set of fin parameters both computationally [1, 2, 5–11] and experimentally [1, 12]. However, no previously published work offered a technique that could take full advantage of these parameters to controllably vector fin thrust at any desired vector – the key focus of this work.

This paper is divided into four parts. First, previous work and the current experimental setup are reviewed. Second, we analyze three major fin gaits

*Corresponding author: John S. Palmisano, Center for Biomolecular Science and Engineering at the Naval Research Laboratory in Washington, DC 20375, USA. E-mail: palmisano@gmail.com.

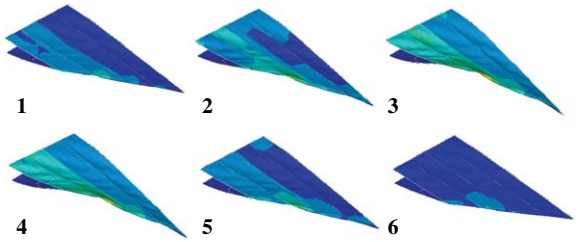

Fig. 1. Fin surface curvature demonstration with FEM stress analysis.

Fig. 2. The NRL robotic pectoral fin with built-in actuators.

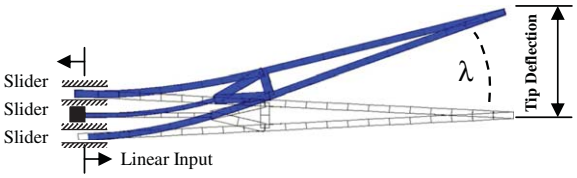

Fig. 3. Rib curvature actuation [1]; pushing/pulling creates curvature as defined by λ, the rib deflection angle.

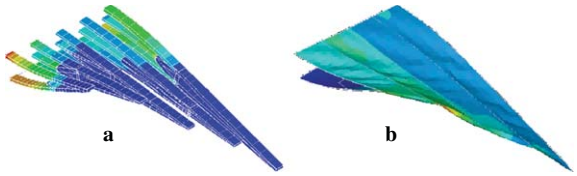

Fig. 4. a) Rib curvature actuation, b) Skin surface flexing FEM: red represents high stress while blue represents low stress. (Colours are visible in the online version of the article; http://dx.doi.org/10.3233/ABB-2012-0064)

separately – forward, reverse, and lift – consisting of preprogrammed kinematics intentionally designed for specific thrust vectors. Third, by combining these main gaits into new and unique sub-gaits, we demonstrate for any desired thrust vector and possible magnitude how to algorithmically create an instant set of matching flapping fin kinematics. Experimental results are given in detail for kinematics, thrust vectors, and thrust magnitudes. Last, we discuss the implications of our fin thrust vectoring method.

2. Previous work and experimental setup

2.1. Background

In our previous study [1] we built a biomimetic controlled-curvature robotic pectoral fin. In that work, we computationally optimized our shape-changing fin using 3D Navier Stokes unsteady computational fluid dynamics (CFD) [5, 10], structural analysis [13], and a control analysis with respect to a UUV [14, 15]. We also performed a full parametric study on pectoral fin design with results experimentally validated [1]. Since those initial studies, we have entirely redesigned our test setup to reduce experimental error and increase data measurement accuracy. For both a quick review of previous work, and a summary of the changes made, the latest experimental setup will now be briefly described.

2.2. Fin design and experimental setup

The experimental setup consists of three major components.

2.2.1. The fin

The first major component is the robotic pectoral fin (see Fig. 2), measuring 11.5 cm long 5.4 cm wide and 8 mm thick at the root. Parts are produced in ABS plastic using a 3D printer (Dimension SST), and the skin is made from silicon rubber (see [1]). The individual ribs used to create the surface curvature are actuated using four Futaba S3114 micro hobby servos, while the bulk rotation (flapping) uses a Hitec HSR-5995TG hobby servo. Servos are waterproofed by coating the internal electronics with electronics-grade RTV and by injecting mineral oil into the gearbox. The fin as a whole requires about two hours for assembly. A 6 V 4500 mA NiMH battery powers the system. See [1] for further fin design details.

The fin produces thrust by flapping and changing shape according to predefined kinematics [1]. Each

rib in the fin, uniquely designed through structural optimization [13], bends by push-pull motions from servos as shown in Fig. 3. Figure 4a demonstrates how multiple ribs combined together can create a desired fin surface curvature. Figure 4b shows how adding skin creates the smooth fin surface.

2.2.2. *The gantry, sensors, and control electronics*

The fin is attached to a gantry-like force measurement device. The device is designed so that the fin can remain deeply submerged underwater, yet still transfer thrust and lift forces to expensive non-waterproofed torque sensors located several inches above the water surface (see Fig. 5). This is important as to avoid various phenomena difficult to model in CFD, such as surface level effects and air bubble ingestion.

On the gantry there are two torque sensors each with custom external op-amp amplification. One torque sensor (RTS-50 by Transducer Techniques) measures fin thrust, while a second orthogonal torque sensor (SWS-20 by Transducer Techniques) measures fin lift and rotational moment forces. Thrust and lift from the fin are mechanically amplified and transmitted to the torque sensors by four long vertical pivoting beams. Sensor and actuator wiring is secured to prevent interference with fin movement. Using CAD and FEA, the gantry was designed to be rigid and lightweight so that its movement, inertial resistance, and structural flexing minimally affect force and kinematics measurements. Although the mechanical structure introduced minimal 'slop' in the torque measurements – filtering out only the higher frequency force variations – our previous work [14] determined that high frequency thrust variations are considered irrelevant in terms of propulsion and control of a fin-propelled UUV.

A 16 MHz ATmega2560 microcontroller is used to not only control all fin servos but also simultaneously collect all sensor data at a rate of ∼50 Hz. The time-stamped data is uploaded in real-time to a PC by USB for storage and analysis. As mentioned in our previous work [1], this microcontroller provides significantly more processing power than is required to operate all aspects of our pectoral fin.

2.2.3. *The water tank*

The gantry device is mounted onto a large 1600 liter all glass water tank (see Fig. 6) measuring 0.71 m × 0.61 m × 2.96 m. A CFD study has shown that this boundary does not affect results by more than

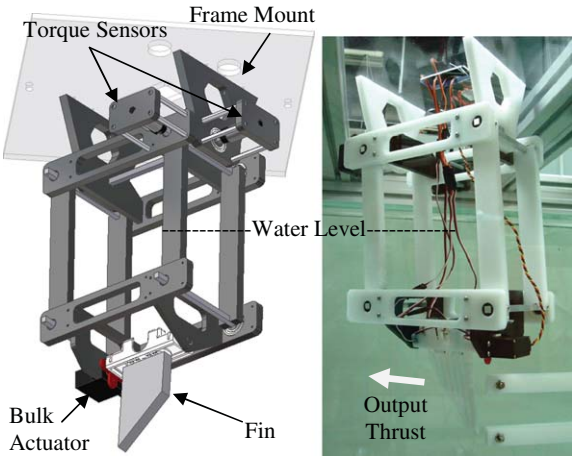

Fig. 5. Gantry fin forces measurement device.

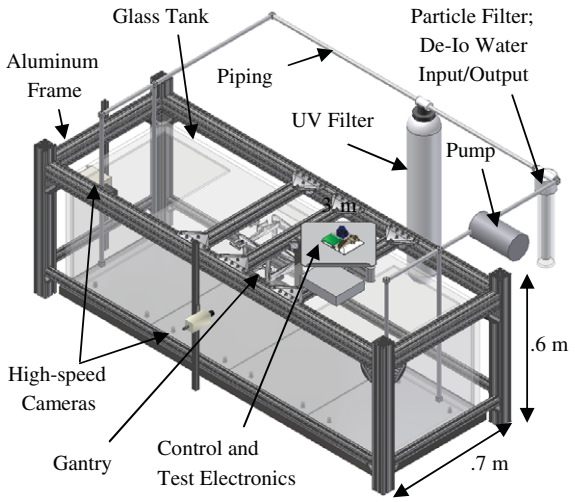

Fig. 6. CAD view of experimental tank setup.

5% (compared to a hypothetical infinite boundary condition). Bio-film growth on both the fin and gantry can negatively affect results by increasing surface drag [16] and possibly modifying other material properties. To prevent this growth, and as a precaution against accidental electrical shorting, de-ionized water is pumped through both a particle filter and a UV light filter before being used to fill the tank. The lab room windows are 100% blacked out from sunlight as an additional precaution against photosynthetic algae blooms – a problem in early testing. Chemical treatments, such as algaecide, were never used.

3. Thrust vectoring generator

3.1. The need for a thrust vectoring generator

Given any set of fin kinematics, output thrust can be determined both experimentally through force measurement sensors and computationally using unsteady CFD. However, the inverse is an entirely different problem: given any desired propulsion vector and average magnitude, what are the required fin motions needed to produce it?

The problem is quite similar to the well-studied inverse kinematics problem for robotic arms. However, unlike with robotic arms, the solution requires solving for non-linear viscous forces using unsteady CFD – dramatically increasing the required computational time. To further complicate the inverse kinematics problem, there are similar issues such as multiple solutions, zero solutions, and singularities to account for. Most importantly, a controller is needed for mobile robots with limited processing capabilities in semi-predictable yet rapidly changing environments – the flying/swimming robot cannot just 'stop' to recalculate a 'perfect' solution within an internal simulation. As such, the controller must have an update rate of at least several cycles per second and must sacrifice accuracy to decrease computation time.

Our proposed pectoral fin thrust vectoring method quickly calculates inverse kinematics by intelligently combining multiple proven pre-selected gaits based on trends found in experimental and CFD results.

3.2. Kinematics

Kinematics is defined as the position of all actuators with respect to time during a single fin flap. Early prototype kinematics [1] were inspired by actual measurements from the Bird Wrasse [17]. Now, kinematics development is results driven – based extensively on experimental data and CFD analysis. After subjectively varying kinematics in experiments and in CFD, collected force data was then used to evaluate the effectiveness of the new kinematics sets for each desired gait.

Kinematics sets are stored as simple arrays in software (see Fig. 7 for an example code snippet). Each array (row) represents an actuator, each column represents a time interval, and each data point represents an actuator control angle. Each column is accessed at a set time interval based on a timer, thereby

```
// programmed kinematics set for lift gait, Kb[t]
Rib_1[7]={100,-60,-60,-60,-60,-60,0,100};
Rib_2[7]={-50,-30,-20,-20,-20,-20,-30,-50};
Rib_4[7]={-50,30,20,20,20,20,0,-50};
Rib_5[7]={70,45,40,35,35,35,40,70};
Bulk_[7]={-100,-90,-62,-22,22,62,90,100};
```

Fig. 7. Example software snippet for lift kinematics. Rows are individual actuators, columns are time steps, and data points represent servo degrees in % of max angle. Commanded angle does not equal performed angle.

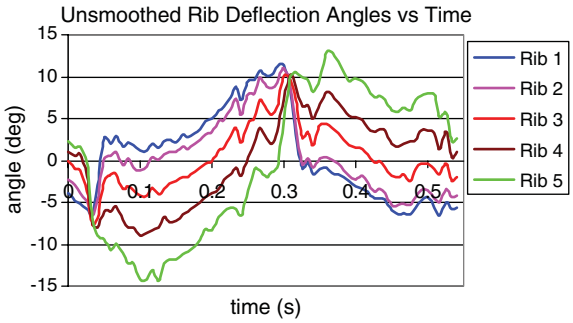

Fig. 8. Unsmoothed rib kinematics, plotting deflection angle vs. time.

coordinating the actuators to move to their prescribed positions.

The total number of positions stored within a kinematics set was chosen based on three factors:

1) The data points must accurately represent the required fin motions (see Figs. 13, 15 and 17). Too few selected points on a curve would misrepresent that curve.
2) Servo motions must not be jerky and should smoothly transition between each time position. 'Position jumping,' sudden movements from one defined position to the next, is a problem inherent for lower fin flapping frequencies as the time between jumps is longer.
3) Since all data points are manually entered and tested, a significant amount of labor is required to program each kinematics set. Too many data points would be prohibitively time-consuming to incorporate.

Based on these above considerations, a balance is required between having too few and too many data points. We hardcoded 8 key points along the curve, and the system automatically interpolates additional points depending on flapping frequency to smoothen motions. For example, at 5 Hz, our system interpolated

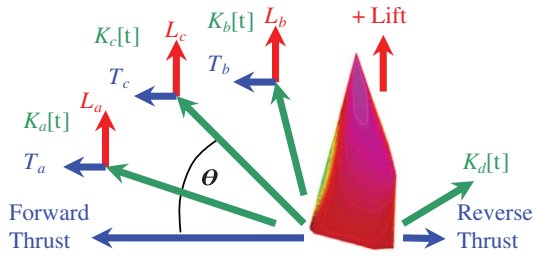

Fig. 9. Pectoral fin with different propulsion vectors.

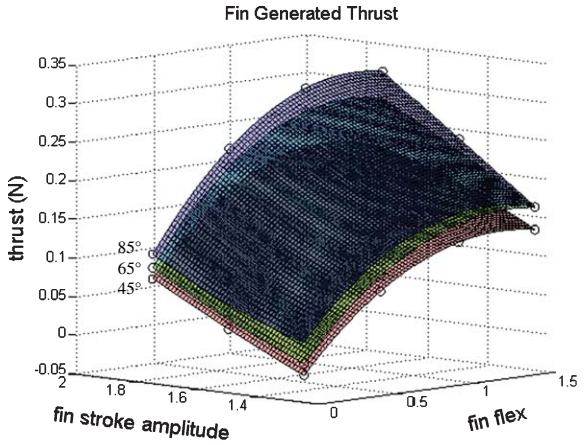

Fig. 10. The effects of weight amplification on average thrust [15]. Layers represent max bulk rotation angle; from top: 85°, 65°, 45°. X and Y-axis values are unit-less scaling multipliers.

an additional 10 curve-fitting points for a total of 20 per flap. At 2 Hz, our system used 80 points, where 70 per flap were interpolated. As an optional alternative to using discrete points, more computationally expensive curve-fitting equations could be used to improve resolution. However, this technique is beyond the scope of this paper and has not been investigated.

Experimental kinematics are measured in 3D by using two orthogonal high-speed digital video cameras (Fig. 6) running at ~60 Hz, and 3D trajectories were extracted using MATLAB as described in [18]. Additional information on the camera setup can be found in [1] and [18]. The experimental fin kinematics (Fig. 8), extracted using the high-speed cameras, consist of rib tip positions recorded throughout the fin stroke. In CFD, this position data is differentiated with respect to time twice to determine the fin accelerations which directly affect fin force output. Differentiating discrete position data, which inherently has some measurement error, produces very noisy velocity and acceleration calculations for the fin. These accelerations must be smoothed to better represent the true experimental fin motions, enabling CFD computations to yield an accurate force time-history curve for the given fin gait (compare Figs. 8 to 13).

3.3. Gaits

Figure 7 is an example of a fin *gait*: a specific preprogrammed kinematics set designed for a single mode of thrust. Different gaits are required for different thrust vectors. For a pectoral fin propelled UUV, the three most important gaits are forward thrust, reverse thrust, and lift. Negative lift (downward force) has been omitted from our study to keep this paper succinct. To note, at a 0° fin angle of attack, negative lift would be the kinematic mirror image of positive lift.

Knowing that gaits can be preprogrammed, it may appear plausible that preprogramming an extensive 'gait database' would be an effective control solution for a pectoral fin. However, entering gaits for all possible thrust vectors into such a database would be far from feasible. Any attempt would result in a stepped control system lacking smooth transitions between gaits. It would also be highly cumbersome to repeatedly create and modify during the prototyping stage. As a solution to the gait database problem, our proposed method algorithmically calculates any gait 'on the fly.' The method is called the Weighted Gait Combination method, or WGC.

3.4. Weighted gait combination method

Suppose a fin control system, on a notional pectoral fin propelled UUV [14, 15], calls for maximum forward thrust (see example in Fig. 9). To do this, the forward thrust gait with kinematics K_a will be used. Or suppose the control algorithm calls for maximum lift, then the lift gait using kinematics K_b would be used. Similarly K_d would be for maximum reverse. Now suppose the controller calls for θ degrees of thrust between full thrust and full lift. An entirely new and unknown set of kinematics, K_c, would be required – yet there are no kinematics sets preprogrammed to choose from.

Using the WGC method, the controller would then algorithmically combine gaits K_a and K_b to create a new hybrid gait, K_c. As a simplified example, Equation (1) shows how two gaits can be averaged together. The rib angles at each time-step t are accessed one at a time from each preprogrammed gait (such as in Fig. 7) and

the result is stored into the arrays of the hybrid gait, K_c.

$$\frac{K_a[t] + K_b[t]}{2} = K_c[t] \tag{1}$$

However, Equation (1) does not allow for an infinitely diverse set of motions. Also, K_a and K_b are usually not 'pure', containing both lift and thrust components. Therefore a weighted percentage term, w, must be used to combine gaits. Since average thrust vector magnitudes of all gaits are typically unequal (Fig. 20), a different weighting must be assigned for each gait as shown in Equation (2).

$$K_a[t]w_a + K_b[t]w_b = K_c[t] \tag{2}$$

To solve for both w_a and w_b, one must assume that the sum of all weights equal an arbitrary total, for example 100% as shown in Equation (3).

$$w_a + w_b = 1 \tag{3}$$

Figure 9 and Equation (2) were used to derive Equations (4) and (5). Basic trigonometry from Fig. 9 was used to derive Equation (6). T_a, T_b, and T_c are average thrust magnitudes of K_a[t], K_b[t], and K_c[t] respectively. Similarly, L_a, L_b, and L_c are average lift magnitudes. T_a, T_b, L_a, and L_b are system-dependent constants that are determined experimentally a-priori such as in section IV. θ is the desired thrust vector for K_c[t], and is used as the control variable. These equations are valid regardless of fin angle of attack.

$$T_a w_a + T_b w_b = T_c \tag{4}$$

$$L_a w_a + L_b w_b = L_c \tag{5}$$

$$\tan(\theta) = \frac{L_c}{T_c} \tag{6}$$

Equations (7) and (8), directly derived from Equations (3–6), are solutions for both weights w_a and w_b. By using Equations (2), (7), and (8), a kinematics set can be calculated for a propulsion vector at any given θ.

$$w_a = \frac{L_b - T_b \tan(\theta)}{(T_a - T_b)\tan(\theta) - L_a + L_b} \tag{7}$$

$$w_b = 1 - \frac{L_b - T_b \tan(\theta)}{(T_a - T_b)\tan(\theta) - L_a + L_b} \tag{8}$$

3.5. Weight amplification

Unlike in Equation (3), the total weight does not need to add up to 100%. By reducing or increasing the total weight percentage by using scale factors, the total output thrust will also be reduced or increased respectively [11, 15]. For supporting evidence, CFD calculated thrust surfaces corresponding to weight amplification are shown in Fig. 10. Because increasing the total weight amplification increases the bending deflection magnitude of a rib, and over-bending will result in material failure, the maximum total weight amplification is limited to this real-world physical constraint.

4. Results

4.1. Center of pressure (CoP)

Locating the fin center of pressure (CoP) is important for determining the moment arm length about the fin rotational axis. By knowing the moment arm length, lift and thrust forces (Fig. 9) can be derived from their respective torque sensors (Fig. 5). Because it is not yet

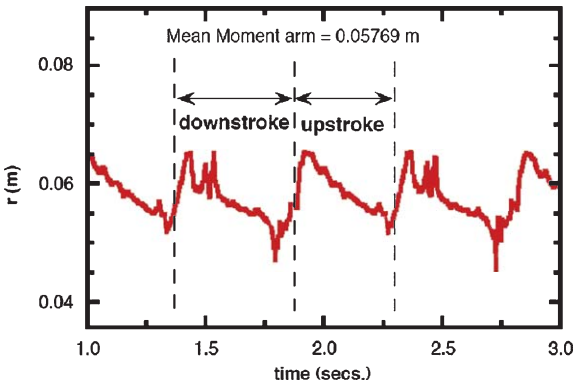

Fig. 11. Typical moving center of pressure for forward thrust gait.

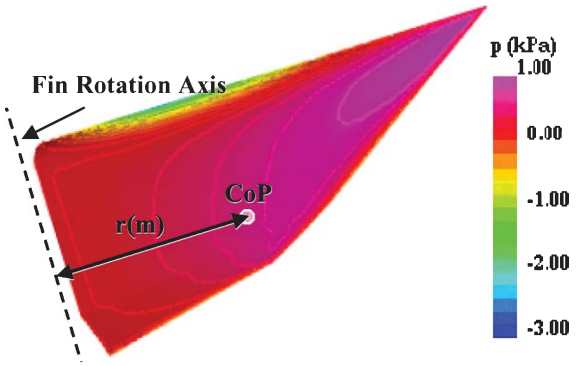

Fig. 12. CFD calculated fin pressure distribution. The distance between the CoP and fin rotation axis is the moment arm length.

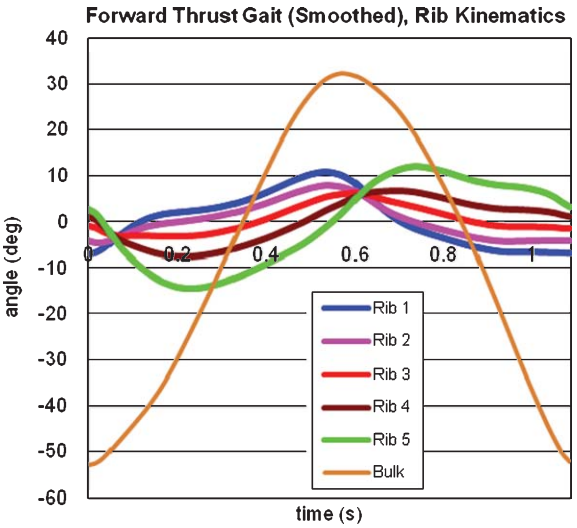

Fig. 13. Experimentally measured forward thrust gait for a single fin stroke, plotted as rib deflection angles λ versus time.

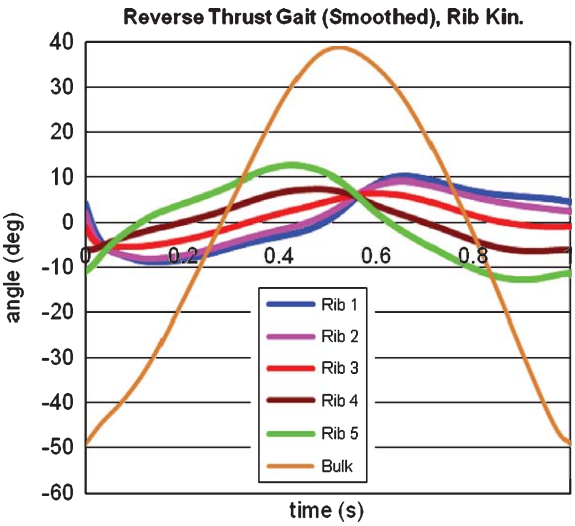

Fig. 15. Experimentally measured reverse thrust gait for a single fin stroke, plotted as rib deflection angles λ versus time.

possible to experimentally determine the time-varying CoP on a flapping fin, experimental fin kinematics data was collected and used in 3D unsteady CFD for analysis. The computed unsteady pressure distribution time-history was then integrated throughout the course of the computation to develop the time-varied location of the CoP. The CoP for the forward thrust gait, specified as a distance away from the fin rotation axis r(m), is plotted over time in Fig. 11. Variation in the CoP is minimal, therefore justifying the use of the average CoP for experimental calculations.

An example fin pressure distribution can be seen in Fig. 12. The average CoP distance from the fin rotation axis, r(m), is 6 cm. Maximum variation from average CoP on the x-axis, which is perpendicular to r(m), is under ∼0.35 cm. Average variation from the CoP is ∼0.6 cm.

4.2. *Forward thrust gait*

The forward gait, using kinematics set $K_a[t]$ as plotted in Fig. 13, was designed to generate maximum forward thrust with minimal wasteful lift force amplitude [1]. Thrust and lift results over several strokes are shown in Fig. 14. Averaged over multiple fin strokes, thrust is 0.16 N, lift is 0.03 N, and power consumption is 15.2 W.

4.3. *Reverse thrust gait*

To our knowledge, this paper is the first that has quantitatively identified the pectoral fin kinematics and corresponding output forces for reverse and lift fin thrust vectoring. Previous pectoral fin propulsion studies have strived to minimize, or entirely ignored, all

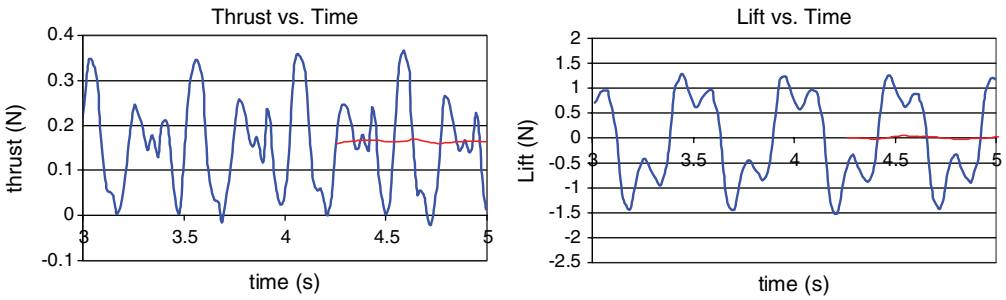

Fig. 14. Thrust and lift results for forward thrust gait.

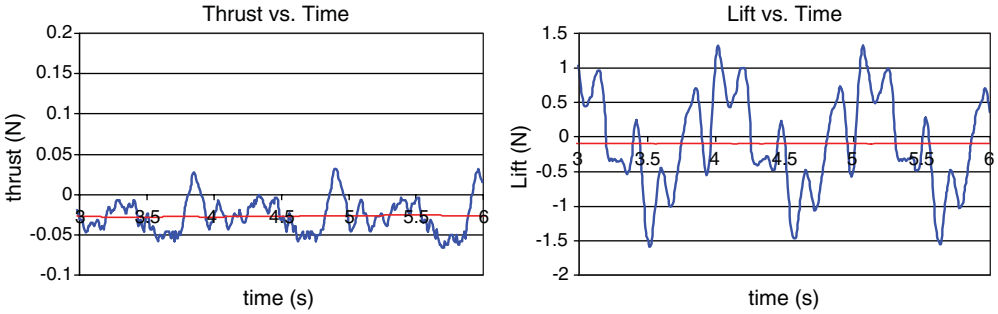

Fig. 16. Thrust and lift results for reverse thrust gait.

other thrust vectors beyond forward thrust – a major mistake if the pectoral fin is to be used as a UUV propulsion and control stability mechanism.

Having no previous literature to guide us, early trial and error attempts to produce significant reverse thrust with our pectoral fin were surprisingly difficult. The reason, we theorize, is because different fin shapes are optimal for different thrust vectors. Our fin had been designed with a high aspect ratio (AR) of 4.5 as previous literature suggested it would maximize forward thrust [1, 3, 10, 19, 20]. However, there is no literature to suggest how AR affects propulsion controllability – the ability to effectively vector thrust in all directions. It is important to know that if a pectoral fin is only optimized for forward thrust, its control capabilities for effective reverse and lift thrust vectoring could be unintentionally crippled.

Why was reverse thrust so difficult to achieve with our fin design? Our previous research and others have confirmed that the most dominating feature on a pectoral fin with respect to forward thrust generation is the leading edge curvature [2, 10, 21]. When generating forward thrust, the leading edge is much longer than the trailing edge (see Fig. 2). But for a fin producing reverse thrust, the opposite is true as the much shorter trailing edge has now become the leading edge. As such, this new short leading edge likely cannot perform nearly as well as the longer leading front edge. As the flow direction is different, the manner is which is passes over the fin will also be different. As pectoral fins are optimized based on many other parameters beyond forward thrust [3, 19, 20, 22], further research must be done to better understand how fin shape affects control and propulsion.

To compensate for the shorter leading edge, our fin uses weight amplification (such as in Fig. 10) to

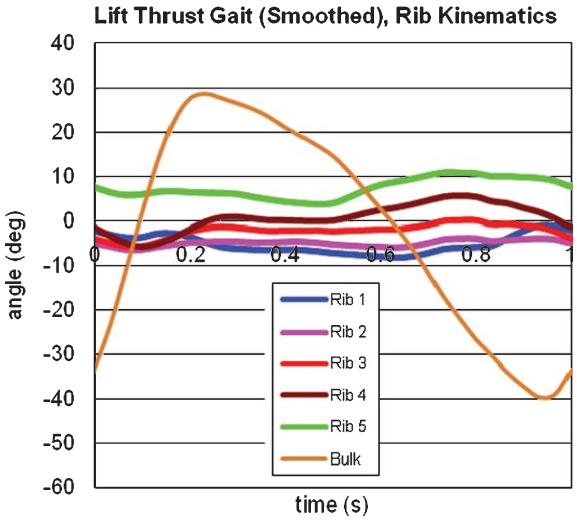

Fig. 17. Experimentally measured lift gait for a single fin stroke, plotted as rib deflection angles λ versus time.

increase reverse thrust. Our reverse thrust gait, designed for maximum negative thrust, is shown in Fig. 15. Thrust and lift results are shown in Fig. 16. Averaged over multiple fin strokes, thrust is negative 0.05 N, lift is 0.00 N, and power consumption is 8.96 W.

4.4. Lift gait

Lift forces on a UUV are required for rising, diving, and rolling motions, and additionally for resisting external vertical environmental disturbances. For a pectoral fin propelled UUV, we separate lift into two types: average lift, and oscillatory lift.

As a fin flaps up and down, lift forces continuously change over time (Fig. 19). The average lift magni-

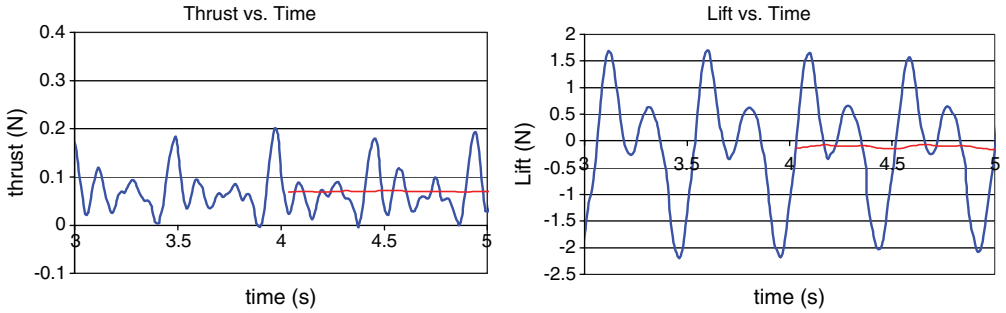

Fig. 18. Thrust and lift results for lift gait.

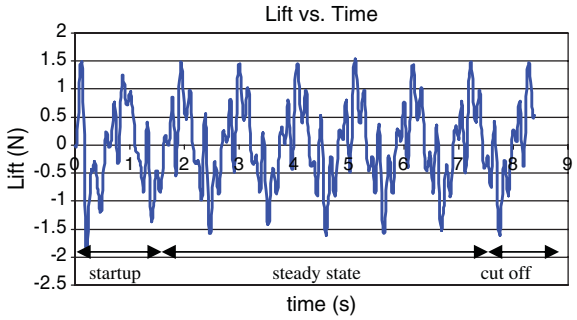

Fig. 19. Lift force plotted over time through many fin strokes. Steady state is achieved in less than one full fin stroke.

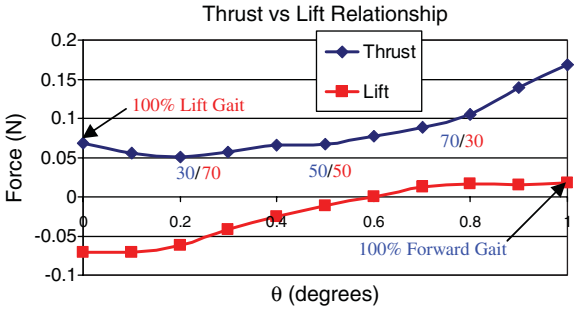

Fig. 20. Average thrust and lift forces plotted as fin transitions from using only the Forward Thrust gait (right) to using only the Lift gait (left).

tude represents the productive work capacity, while the peak-to-peak amplitude of those forces represents oscillatory lift. Oscillatory lift, inherent and unavoidable in any flapping fin actuator, wastefully saps energy and creates control instability – thereby degrading system performance. This is a major reason why rigid fins, known to have higher amplitude oscillatory lift [2, 21], cannot perform as effectively as flexible controlled-curvature fins.

Our gait designed for maximum average lift magnitude is shown in Fig. 17, with thrust results over several strokes shown in Fig. 18. Averaged over multiple fin strokes, forward thrust is 0.07 N, lift is −0.1 N, and power consumption is 10.7 W.

4.5. Steady state and gait transition time

The pectoral fin, with every gait we tested, reached the equivalent of steady state within one full stroke (see Fig. 19). This result demonstrates the high experimental reliability of our robotic pectoral fin. Averaged data is collected only during steady state, ignoring the initial startup fin stroke where data could be unreliable.

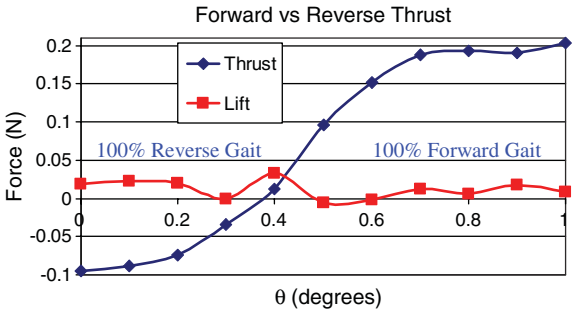

Fig. 21. Average thrust and lift forces plotted as fin transitions from using only the Reverse Thrust gait (left) to using only the Forward gait (right).

As such, we conclude that a full effective gait transition can be completed within a single stroke.

4.6. Weighted gait combinations

To demonstrate that the WGC method can predictably vector thrust, both thrust and lift forces were measured simultaneously as the gait was transitioned

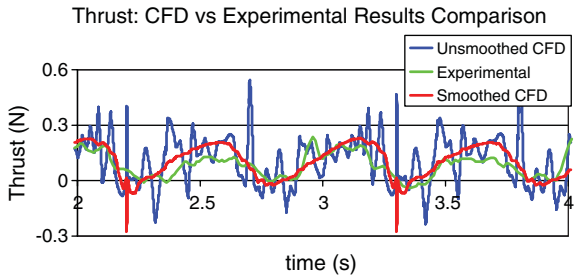

Fig. 22. Comparing CFD results to Experimental results for thrust.

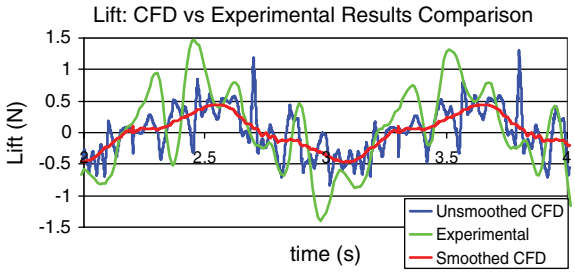

Fig. 23. Comparing CFD results to Experimental results for lift.

from full lift to full thrust. Figure 20 plots the average force magnitudes over this transition. As the control variable θ is increased, forward thrust increases while lift generally decreases – validating WGC as an effective pectoral fin thrust vectoring method.

We explored using WGC for velocity control by mixing the Forward and Reverse gaits. Figure 21 shows a sinusoidal trend between forward and reverse thrust, with intermediate speeds during the transition, verifying that WGC can be used as a velocity control method. No trends in power consumption were identified over any WGC transition. Note that the transition characteristics will greatly vary depending on kinematics, flapping speed, and total bulk angle. Kinematics that will achieve maximum thrust and lift kinematics must be used, or the transition between the two mixed gaits could become unusable for the WGC method.

4.7. Experimental vs. CFD results comparison

CFD can be used as an exploratory tool to both guide theory and predict experimental results. Although our CFD method has already been validated for hovering fruit flies [23, 24] and swimming fishes [5], it is necessary to validate the CFD accuracy in comparison to measured experimental results for this particular fin design. Figures 22 and 23 show three force curves for the same fin experiment. The green curve shows sensor data collected experimentally. The blue curve represents CFD results computed from raw unsmoothed kinematics data. Lastly, the red force curve is generated by smoothing out the raw kinematics data for a second CFD simulation.

The experimental results provide a more accurate representation of the fin-generated forces since the parameters used in the CFD simulation do not account for fluid structure interaction. Although local peak-to-peak amplitudes vary for each curve, the experimental moving average has been accurately captured by the CFD results. Originally, there were concerns that these large peak-to-peak amplitudes over the course of a single fin stroke could negatively affect the maneuvering response of a notional pectoral fin-propelled UUV. However, simulation results demonstrate that the inertial response of our vehicle is sufficiently damped, yielding only small angle oscillations induced by the high frequency flapping. Therefore using only the averaged thrust of a stroke is sufficient for stable UUV control [14]. While modeling only approximate peak-to-peak force data is necessary for a controls simulation, more accurate data is required for mechanical design and component failure prevention.

5. Extended applications, discussion

5.1. WGC for other robots: Beyond fish

We hypothesize that the WGC method, independent of the mechanism involved, can be used to control many other hyper-complex robots with large numbers of interdependent degrees of freedom (DOF). Assuming the transition gaits are stable, this would include bipeds, snakes, hexapods, etc. By pre-programming a handful of optimized gates (running, jumping, jogging, backwards walking, side-stepping, etc), then performing the WGC method, a highly adaptable range of motions could be created.

5.2. Non-linear WGC

The WGC method as described in this paper treats the transition between K_a and K_b as linear. Although not linear, results in Figs. 20, 21 can be approximated

as a linear system. By treating the system as linear it reduces both the computational burden on a UUV microcontroller, and avoids the more detailed and time intensive experimentation needed to accurately model the system. Being outside the scope of this paper, a non-linear weighting adjustment method was not pursued.

5.3. On genetic algorithms

Performing a genetic algorithm computationally for a controlled-curvature pectoral fin is entirely infeasible with modern-day computers. To compute the force profile for several flapping cycles, a single fin gait consisting of 6 DOF (5 actuators in a time dependent domain) would take ∼1.5 days on our 8 processor SGI Altix computer. Because thousands of gaits must be analyzed to find a good solution, years of computing time would be required. The literature supports this conclusion that CFD computation of controlled-curvature pectoral fins is time/processor intensive [1, 3, 21] and that a genetic algorithm using CFD is perhaps prohibitively so [25].

Another option is to experimentally run a genetic algorithm. Approximately one minute is required to experimentally test and process a gait, therefore a comprehensive set of gaits could be tested within weeks. The disadvantage is that a working device must already be built and perform reliably without failure over a large number of cycles. The sensors must also not drift in calibration over that period of time.

The solutions gained from the genetic algorithm, whether experimentally or computationally, would then be stored in a gait database. However, any mechanical design modification would invalidate the database thereby forcing a full recalculation. At the prototyping stage, this is unacceptable.

We propose that if a genetic algorithm is to be performed, it should only solve for the major gaits (forward, reverse, lift, etc.) and then use the results with the WGC method to create the additional intermediate gaits.

5.4. On efficiency

For this paper, neither the gaits nor the electromechanical setup were designed with efficiency in mind. Research is currently being performed to study the relationship of pectoral fin gaits with respect to efficiency.

5.5. On wasteful oscillation

While counter-productive thrust can be made negligible through careful kinematics design, wasteful oscillatory lift is both inherent and significant in dorso-ventral flapping fin propulsion. As such, reducing non-productive oscillatory thrust and lift will improve system performance. We hypothesize that modifying the fin angle of attack throughout the fin stroke can productively redirect otherwise wasteful oscillatory propulsion forces. However, control over fin angle of attack has not been attempted due to the required increase in fin mechanical complexity. We hypothesize that a control system, using external flow sensors in a feedback loop, has the potential to harness oscillatory forces as a way to mitigate external environmental disturbances and/or enhance thrust.

5.6. On PID

A major advantage of the WGC method is in its linearity and simplicity – it easily lends itself to fuzzy logic PID control with the single control variable, θ. In related research we have shown in simulation that a UUV, driven differentially by two pectoral fins on either side using WGC, is more stable than when using the 'gait database' method [15].

5.7. On external flow

Experimentally, gaits were validated in our test tank in static water – in absence of an applied external flow. As the fin was designed and the gaits were selected for performance in external flow on an UUV, we studied and validated each gait under various realistic flow conditions using CFD coupled with vehicle-level controls simulations [11, 15]. Assuming a sensing capability to determine flow was added directly onto or near the pectoral fin [26, 27], it would be possible to expand WGC to incorporate additional preprogrammed optimal gaits for any typical external flow.

5.8. Lateral forces

This work considered only fin lift and fin thrust vectors for propulsion. Although lateral forces exist as determined through our CFD analyses, they are mostly negligible on a UUV as the opposing lateral forces from the opposite fin generally cancels it out. There are situations in which a UUV can be affected (both positively

and negatively) by lateral forces, but is out of scope of this paper. Current research is addressing the effective use and control of lateral forces.

6. Conclusion

A method of rapidly creating pectoral fin gaits for controlled thrust vectoring has been devised. A limited set of kinematics for major propulsion modes were created and tested, then algorithmically combined into a non-computationally intensive controller of weighted gait combinations. By using this experimentally and computationally validated technique, a pectoral fin actuator can be used to give 6 DoF controllability to a UUV.

Acknowledgments

Special thanks to Tewodros Mengesha at George Washington University for his continued 3D prototyping support, Kerr-Jia Lu for the FEM stress analysis of the fin, and Eric Sumner for his assistance in the gantry design. Additional thanks to members at societyofrobots.com/robotforum for technical support.

References

[1] J. Palmisano, R. Ramamurti, K.J. Lu, J. Cohen, W.C. Sandberg and B. Ratna, Design of a Biomimetic Controlled-Curvature Robotic Pectoral Fin, *2007 IEEE Int Conf on Robotics and Automation*, Roma, Italy, 2007, pp. 966–973.

[2] R. Ramamurti and W.C. Sandberg, The influence of fin rigidity and gusts on force production in fishes and insects: A computational study, *42nd AIAA Aerospace Sciences Meeting*, AIAA 2004-404, January 2004.

[3] S. Combes and T. Daniel, Shape, Flapping and Flexion: Wing and Fin Design for Forward Flight, *The Journal of Experimental Biology* **204** (2001), 2073–2085.

[4] G. Lauder and P. Madden, Learning from Fish: Kinematics and Experimental Hydrodynamics for Roboticists, *International Journal of Automation and Computing* **4** (2006), 325–335.

[5] R. Ramamurti, W.C. Sandberg, R. Löhner, J. Walker and M. Westneat, Fluid dynamics of flapping aquatic flight in the bird wrasse: Three-dimensional unsteady computations with fin deformation, *Journal of Experimental Biology* **205** (2002), 2997–3008.

[6] R. Ramamurti, R. Löhner and W.C. Sandberg, Computation of 3-D Unsteady Flow Past a Tuna with Caudal Fin Oscillation, *Advances in Fluid Mechanics* **9**, (ed. M. Rahman and C.A. Brebbia), Southhampton, UK, Computational Mechanics Publications, 1996, pp. 169–178.

[7] W.C. Sandberg and R. Ramamurti, Unsteady Flow Computational Technology for Flapping Fins, *Proc Unmanned Undersea Submersibles Technology Symposium*, Durham, NH, Autonomous Systems Institute, 1999, pp. 182–194.

[8] R. Ramamurti, R. Löhner, and W.C. Sandberg, Computation of the 3-D Unsteady Flow Past Deforming Geometries, *Intl J Comp Fluid Dynamics* **13** (1999), 83–99.

[9] R. Ramamurti and W.C. Sandberg, Simulation of the Flow about Flapping Airfoils Using a Finite-Element Incompressible Flow Solver, *AIAA Journal* **39** (2001), 253–260.

[10] R. Ramamurti and W.C. Sandberg, Computational Fluid Dynamics Study for Optimization of a Fin Design, *24th AIAA Applied Aerodynamics Conference*, AIAA-2006–3658, 2006.

[11] R. Ramamurti, W.C. Sandberg, J. Geder and J. Palmisano, Computations of Flapping Fin Propulsion for UUV Design, 47th AIAA Aerospace Sciences Conference, January 2009.

[12] J. Tangorra, S.N. Davidson, I. Hunter, P. Madden, G. Lauder, H. Dong, M. Bozkurttas and R. Mittal, The Development of a Biologically Inspired Propulsor for Unmanned Underwater Vehicles, *IEEE Journal of Oceanic Engineering* **32**(3), 2007.

[13] B.P. Trease, K.J. Lu and S. Kota, Biomimetic Compliant System for Smart Actuator-Driven Aquatic Propulsion: Preliminary Results, ASME Int. Mechanical Eng. Congress & Exposition, Washington, D.C., IMECE2003-41446, 2003, pp. 43–52.

[14] J. Geder, J. Palmisano, R. Ramamurti, W.C. Sandberg and B. Ratna, A New Hybrid Approach to Dynamic Modeling and Control Design for a Pectoral Fin Propelled UUV, *15th International Symposium on Unmanned Untethered Submersible Technology*, Durham, New Hampshire, USA on August 19th-22nd, 2007.

[15] J. Geder, J. Palmisano, R. Ramamurti, W.C. Sandberg and B. Ratna, Fuzzy Logic PID Based Control Design and Performance for Pectoral Fin Propelled Unmanned Underwater Vehicle, International Conference on Control, Automation, and Systems, Seoul, Korea on October 14–17, 2008, pp. 40–46.

[16] M. Schultz and G. Swain, The Influence of Biofilms on Skin Friction Drag, *Biofouling* **15**(1-3) (2000), 129–139.

[17] J. Walker and M.A. Westneat, Labriform propulsion in fishes: Kinematics of flapping aquatic flight in the bird wrasse, Gomphosus varius, *Journal of Experimental Biology* **200** (1997), 1549–1569.

[18] J. Geder, W.C. Sandberg and R. Ramamurti, Multi-Camera, High-Speed Imaging System for Kinematics Data Collection, Naval Research Laboratory Memorandum Report NRL/MR 6401-07-9054, September, 2007, pp. 1–9.

[19] P. Wainwright, D. Bellwood and M. Westneat, Ecomorphology of Locomotion in Labrid Fishes, *Environmental Biology of Fishes* **65** (2002), 47–62.

[20] J. Walker and M. Westneat, Performance limits of labriform propulsion and correlates with fin shape and motion, *The Journal of Experimental Biology* **205** (2002), 177–187.

[21] G. Lauder, P. Madden, I. Hunter, J. Tangorra, N. Davidson, L. Proctor, R. Mittal, H. Dong and M. Bozkurttas, Design and Performance of a Fish Fin-Like Propulsor for AUVs, The 14th International Symposium on Unmanned Untethered Submersible Technology, Lee, New Hampshire, USA, 2005.

[22] D. Collar, P. Wainwright and M. Alfaro, Integrated diversification of locomotion and feeding in labrid fishes, *Biology Letters* **4** (2008), 84–86.

[23] R. Ramamurti and W.C. Sandburg, A three-dimensional computational study of the aerodynamic mechanisms of insect flight, *Journal of Experimental Biology* **205**(10) (2002), 1507–1518.

[24] R. Ramamurti and W.C. Sandburg, A computational investigation of the 3-D unsteady aerodynamics of Drosophila hovering and maneuvering, *Journal of Experimental Biology* **210**(5) (2007), 881–896.

[25] D. Knight, Automated Optimal Design Using CFD and High Performance Computing, *Lecture Notes in Computer Science* **1215** (1996), 198–221.

[26] S. Coombs, Smart Skins: Information Processing by Lateral Line Flow Sensors, *Autonomous Robots* **11** (2001), 255–261.

[27] Z. Fan, J. Chen, J. Zou, D. Bullen, C. Liu and F. Delcomyn, Design and fabrication of artificial lateral line flow sensors, *Journal of Micromechanics and Microengineering* **12** (2002), 655–661.